PIER C

(Received 15 December 2024, Accepted 3 March 2025, Scheduled 14 March 2025)

Efficient Electro-Thermal Analysis of Periodic Artificial Magnetic Conductors (AMC)

Zhonghui Li, Minquan Li*, Xianliang Wu, Shuangqing Cao, and Rongxian Bai

Information Materials and Intelligent Sensing Laboratory of Anhui Province, Anhui University, Hefei 230039, China

ABSTRACT: This paper proposes a method to calculate temperature distribution by analyzing periodic units, enabling the efficient simulation of electromagnetic-thermal problems in periodic structures. Compared with traditional methods that require high memory and long computation times to process the entire large-scale model, this approach significantly reduces computational complexity by focusing on a single periodic unit and incorporating periodic thermal boundary conditions. In the study, electromagnetic losses are considered as the heat source, and the formula for periodic thermal boundary conditions is derived in conjunction with the heat conduction equation, achieving the integration of periodic electromagnetic-thermal boundary conditions. Numerical validation and comparison with global model results demonstrate that the proposed method maintains accuracy while achieving high efficiency. Furthermore, the method is applied to an artificial magnetic conductor (AMC) model, with calculation results closely matching those of large-scale unit arrays, further verifying the correctness and applicability of the algorithm.

1. INTRODUCTION

The periodic electromagnetic boundary is well established, whereas the periodic thermal boundary is seldom discussed. For structures with periodic distributions, determining the temperature distribution of the entire structure demands considerable memory and extensive computational time. This paper presents a method to derive the temperature distribution of the entire structure by directly analyzing a single periodic element.

ElMahgoub et al. introduced the concepts of arbitrary skewed grids [1] and multilayered periodic structures [2], followed by the development of dispersive periodic boundary conditions [3], marking the foundation of periodic electromagnetic boundary research. Subsequently, researchers proposed staggered grid periodic boundaries [4], while Tekbas et al. provided the analytical solution for infinite medium plates [5].

Currently, the finite element method [6] and spectral element time-domain method [7] are widely employed for heat calculation. To enhance computational efficiency, domain decomposition methods [8] and parallel computing techniques [9, 10] have been adopted. However, existing research on electromagnetic-thermal coupling [11, 12] does not address periodic thermal boundaries.

Unresolved issues with periodic boundary conditions include the following: 1) Periodic electromagnetic boundary conditions are well established, but periodic thermal boundary conditions have been scarcely explored. 2) Periodic boundary conditions can be used to simulate an infinitely large object, where a single unit cell with periodic boundaries can represent the performance trends of the entire structure. However, in thermal analysis, the existing boundary conditions often conflict with periodic thermal conditions. 3) Heat sources generate temperature gradients, which limit the straightforward application of periodic boundary conditions. Therefore, for models composed of arrays of identical unit cells, such as metamaterials and phased array antennas, solving coupled electromagnetic-thermal multiphysics problems for the entire structure requires considerable computational memory and time.

The main contributions of this paper are as follows: 1) The periodic thermal boundary condition is derived from the periodic electromagnetic boundary condition, achieving the integration of periodic electromagnetic-thermal boundary conditions. 2) The existing thermal boundary conditions are improved by integrating periodic thermal boundary conditions with traditional thermal boundary conditions. 3) Electromagnetic losses are used as heat sources, deriving the formula for periodic thermal boundaries through the heat conduction equation. This method allows for calculating the temperature distribution of the entire structure by solving only the periodic unit cell.

In this study, a plane wave is used as the excitation source, and the simulated model requires a periodic structure. When a plane wave propagates through the periodic structure, the electric field distribution within each unit cell becomes identical. As a result, the heat generated in each unit cell leads to a periodic thermal distribution. Electromagnetic-thermal multiphysics coupling [13–16] involves using the electric field in the electromagnetic domain as the heat source in the heat conduction equation. Since the electric field is uniform across the unit cells of the periodic structure, the heat sources within each unit cell remain consistent. Consequently, the thermal distribution of the entire structure can be determined by calculating the heat within a single unit cell and applying periodic thermal boundary conditions.

* Corresponding author: Minquan Li (AHU411MHz@hotmail.com).

2. FORMULATION

The basic finite-difference time-domain (FDTD) iteration (1). The remaining components E_y, E_z, H_x, H_y, H_z, and (1) can be derived using the same approach. Equations (2) and (3) serve as the fundamental formulas for periodic electromagnetic boundary iterations. The remaining components $E_y(1,j,k)$, $E_y(nx+1,j,k)$, $E_z(1,j,k)$, $E_z(nx+1,j,k)$, $E_z(i,1,k)$, and $E_z(i,ny+1,k)$ can be determined straightforwardly. However, $E_z(i,j,k)$ requires special handling at the four corners defined by (4), (5), (6), and (7).

$$E_x^{n+1}(i,j,k) = C_{exe}(i,j,k) \times E_x^n(i,j,k)$$
$$+C_{exhz}(i,j,k)\left[H_z^{n+1/2}(i,j,k) - H_z^{n+1/2}(i,j-1,k)\right]$$
$$+C_{exhy}(i,j,k)\left[H_y^{n+1/2}(i,j,k) - H_y^{n+1/2}(i,j,k-1)\right], \quad (1)$$

$$C_{exe}(i,j,k) = \frac{2\varepsilon_x(i,j,k) - \Delta t\sigma_x^e(i,j,k)}{2\varepsilon_x(i,j,k) + \Delta t\sigma_x^e(i,j,k)},$$

$$C_{exhz}(i,j,k) = \frac{2\Delta t}{(2\varepsilon_x(i,j,k) + \Delta t\sigma_x^e(i,j,k))\Delta y},$$

$$C_{exhy}(i,j,k) = \frac{2\Delta t}{(2\varepsilon_x(i,j,k) + \Delta t\sigma_x^e(i,j,k))\Delta z}.$$

$$E_x^{n+1}(i,1,k) = C_{exe}(i,1,k) \times E_x^n(i,1,k)$$
$$+C_{exhz}(i,1,k)\left[H_z^{n+1/2}(i,1,k) - H_z^{n+1/2}(i,n_y,k)\right.$$
$$\left.\times e^{jk_yP_y}\right] + C_{exhy}(i,1,k)\left[H_y^{n+1/2}(i,1,k)\right.$$
$$\left.-H_y^{n+1/2}(i,1,k-1)\right], \quad (2)$$

$$E_x^{n+1}(i,n_y+1,k) = E_x^{n+1}(i,1,k) \times e^{-jk_yP_y}, \quad (3)$$

where k_y is the propagation constant in the y-direction, and P_y is the length of the simulation model in the y-direction.

$$E_z^{n+1}(1,1,k) = C_{eze}(1,1,k) \times E_z^n(1,1,k) + C_{ezhy}(1,1,k)$$
$$\times\left[H_y^{n+1/2}(1,1,k) - H_y^{n+1/2}(n_x,1,k) \times e^{jk_xP_x}\right]$$
$$+C_{ezhx}(1,1,k) \times \left[H_x^{n+1/2}(1,1,k) - H_x^{n+1/2}(1+S,n_y,k)\right.$$
$$\left.\times e^{jk_yP_y}\right], \quad (4)$$

$$E_z^{n+1}(n_x+1,1,k) = E_z^{n+1}(1,1,k) \times e^{-jk_xP_x}, \quad (5)$$
$$E_z^{n+1}(1,n_y+1,k) = E_z^{n+1}(1+n_x-S,1,k) \times e^{-jk_yP_y}, \quad (6)$$
$$E_z^{n+1}(n_x+1,n_y+1,k) = E_z^{n+1}(1,1,k) \times e^{-jk_xP_x}$$
$$\times e^{-jk_yP_y}. \quad (7)$$

Electromagnetic loss [17] serves as the source of heat generation, and the electromagnetic field is coupled with the thermal field through the heat conduction Equation (8) [18]. The discretization of the heat conduction equation is expressed in (9).

$$\rho c_m \frac{\partial T}{\partial t} = \nabla \cdot (K\nabla T) + \frac{1}{2}\sigma E^2, \quad (8)$$

where ρ is the medium density, c_m the specific heat of the medium, K the thermal conductivity of the medium, E the electric field intensity, and σ the electric conductivity.

$$T^{n+1}(i,j,k) = T^n(i,j,k) + \Delta t_T * \frac{K(i,j,k)}{\rho(i,j,k)c_m(i,j,k)}$$
$$\left(\frac{T^n(i+1,j,k) - 2T^n(i,j,k) + T^n(i-1,j,k)}{\Delta x^2}\right.$$
$$+\frac{T^n(i,j+1,k) - 2T^n(i,j,k) + T^n(i,j-1,k)}{\Delta y^2}$$
$$\left.+\frac{T^n(i,j,k+1) - 2T^n(i,j,k) + T^n(i,j,k-1)}{\Delta z^2}\right)$$
$$+\frac{\Delta t_T}{\rho(i,j,k)c_m(i,j,k)} * P^n(i,j,k), \quad (9)$$

$$P = \frac{1}{2}\sigma E^2, \quad (10)$$

$$\Delta t_T \le \frac{\rho c_m}{2K}\left(\frac{1}{\Delta x^2} + \frac{1}{\Delta y^2} + \frac{1}{\Delta z^2}\right)^{-1}, \quad (11)$$

where n is the current time step, $n+1$ the next time step, and Δt_T the propagation time for each step of the calculated temperature.

Periodic thermal boundaries cannot be updated due to the lack of external grids. For example, updating $T(1, 1:nx, 1:nz)$ requires $T(0, 1:nx, 1:nz)$, but $T(0, 1:nx, 1:nz)$ does not exist. In such cases, the boundary is usually left not updated, but this approach often leads to errors in the results. Here, "$1:nx$" represents all integers from 1 to *nx*.

Before this paper, the calculation of thermal effects in large structural models with periodic structures typically involved first performing electromagnetic modeling and simulation on a single unit cell. Then, the electric field obtained from that unit cell would be distributed to the corresponding positions of each unit in the entire large model to calculate the thermal effects of the whole model. However, this method requires a large amount of time and memory. For the reasons mentioned above, this paper proposes thermal periodic boundaries.

As long as the electric field maintains a periodic arrangement, the thermal calculation of the model can be carried out using the following periodic thermal boundary method. This method only requires the calculation of the smallest periodic unit along with the periodic thermal boundaries to determine the thermal response of the entire model. In this paper, the thermal equivalent is represented at the center of the Yee grid. Here, *nx*, *ny*, and *nz* denote the numbers of grids along the X, Y, and Z axes, respectively.

Explanation of Fig. 1:

1) Assign all heat values at $X = nx$ to the grid at $X = 0$. All heat at $X = 1$ is assigned to the grid at $X = nx + 1$.
2) Assign all heat values at $Y = ny$ to the grid at $Y = 0$. All heat at $Y = 1$ is assigned to the grid at $Y = ny + 1$.

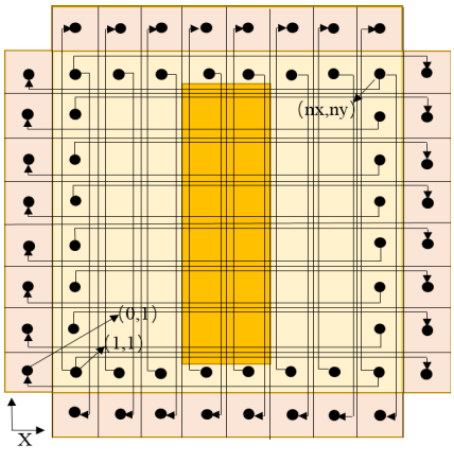

FIGURE 1. Diagram of the thermal periodic boundary update method.

At the beginning of each iteration, the heat assignment operation is performed using the method shown in Fig. 1. Subsequently, the program employs the conventional thermal iteration method for the overall update of the periodic unit, simplifying the programming complexity.

The following describes, in detail, the algorithm combining periodic electromagnetic and thermal boundary conditions: 1) A subunit of the model with a periodic structure is selected, and the electromagnetic field simulation is performed using periodic electromagnetic boundary conditions. 2) Heat generation is assigned according to the method illustrated in Fig. 1. Equations (12) and (13) formalize this method, and as shown in Fig. 1, a similar approach can be applied in the y-direction. 3) The temperature field is updated using the heat conduction Equation (9). 4) Steps 1), 2), and 3) are repeated until the temperature difference between two successive iterations is less than 1%. Fig. 2 presents the flowchart of the algorithm.

In this study, the periodic distribution in the XY planes is explained as an example, and the method can be extended to other planes accordingly.

$$T(0, 2 : ny-1, k) = T(nx, 2 : ny-1, k). \tag{12}$$

$$T(0, 1, k) = T(nx, 1, k). \quad T(1, 0, k) = T(1, ny, k). \tag{13}$$

This study focuses on a periodic distribution on a single plane, simulating an infinitely large plane. Periodic thermal boundary conditions are applied around the four edges of the periodic structural subunit, while standard thermal boundary conditions are applied to the upper and lower surfaces (14).

$$\frac{\partial T}{\partial n} = \frac{h}{K}\left(T_{object} - T_{\mathrm{su}}\right). \quad n = z, \tag{14}$$

where T_{object} is the surface temperature of the measured object, T_{su} the ambient temperature surrounding the measured object, and h the coefficient of heat convection.

3. NUMERICAL EXAMPLE

3.1. Method for Verifying the Correctness of the Algorithm

To validate the correctness of the proposed periodic thermal boundary conditions, we conducted comparative tests using

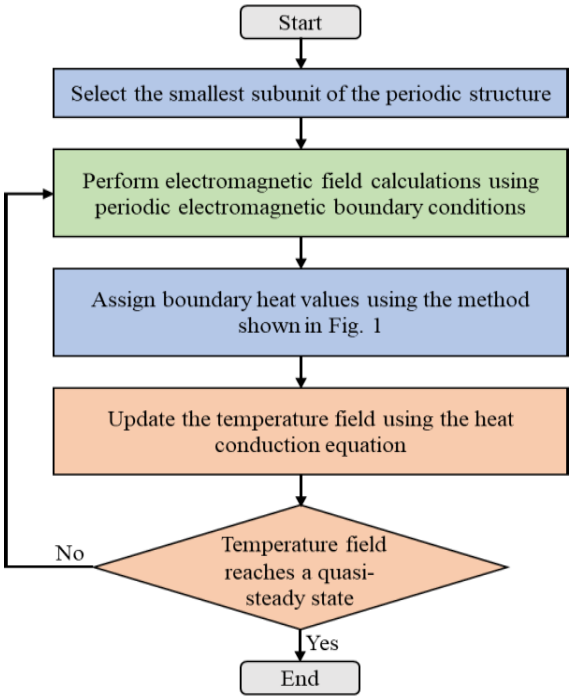

FIGURE 2. Algorithm flowchart combining periodic electromagnetic boundary conditions and periodic thermal boundary conditions.

three different methods. The simulations were performed on two cuboid dielectric materials with specific dimensions and properties.

Case 1: A cuboid with dimensions 102 mm × 102 mm × 9.2 mm, dielectric constant $\varepsilon = 2.56$, and conductivity $\sigma = 0.004$ (referred to as Cuboid 1). Case 2: A smaller cuboid with dimensions 1.6 mm × 1.6 mm × 9.2 mm, dielectric constant $\varepsilon = 2.56$, and conductivity $\sigma = 0.004$ (referred to as Cuboid 2), which can be considered as a periodic unit of Cuboid 1.

1) First Test (Global Model): The electromagnetic field of Cuboid 1 was computed, and the temperature distribution was subsequently calculated using the heat conduction equation. The temperature was sampled at the central region, as shown in Fig. 3. 2) Second Test (Proposed Periodic Thermal Boundary): The electromagnetic field of Cuboid 2 was simulated with periodic electromagnetic boundary conditions. The proposed periodic thermal boundary conditions were applied to the four

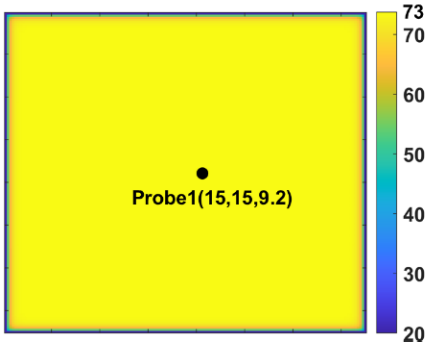

FIGURE 3. Temperature distribution of Cuboid 1 at the top at 21 ns (unit: °C).

lateral surfaces, while thermal boundary conditions were applied to the top and bottom surfaces. The temperature distribution was then calculated using the heat conduction equation. 3) Third Test (Full Thermal Boundaries): Similar to the second test, the electromagnetic field of Cuboid 2 was simulated with periodic electromagnetic boundary conditions. However, thermal boundary conditions were applied to all six surfaces, and the temperature distribution was calculated.

From Fig. 4, the temperature distributions from the first and second tests match perfectly, confirming the validity of the proposed periodic thermal boundary conditions. In contrast, a noticeable discrepancy exists between the results of the first and third tests. These comparative simulations demonstrate that the proposed periodic thermal boundary conditions provide accurate results consistent with the global model.

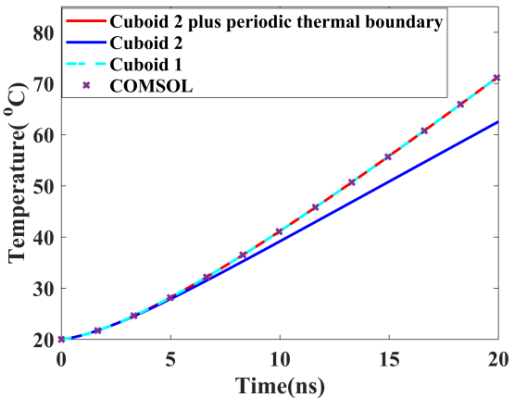

FIGURE 4. The temperature variation with time for three simulation methods.

As shown in Table 1, the computational time and memory required for Cuboid 1 are significantly larger than those for Cuboid 2. The computational time and memory usages for Cuboid 2 with and without the proposed periodic thermal boundary conditions are nearly identical. The results obtained for Cuboid 2 with periodic thermal boundary conditions are consistent with those of Cuboid 1.

TABLE 1. Three simulations use time and memory.

Type	Execution time	Memory
Cuboid 1	74.702 minutes	62923 MB
Cuboid 2	0.08229 minutes	3748 MB
Cuboid 2 plus periodic thermal boundary	0.09479 minutes	3784 MB
COMSOL	97.532 minutes	142687 MB

In this study, a plane wave excitation (TEM mode) was employed, with a sinusoidal waveform of amplitude 5×10^6 V and frequency 8 GHz. The heat transfer coefficient was set to $h = 1.5\,\mathrm{W/m^2 \cdot K^{-1}}$. The electromagnetic and thermal calculations were performed with the same time step, with electromagnetic and thermal fields updated alternately.

3.2. The Combined Simulation of Periodic Electromagnetic Boundary Conditions and Periodic Thermal Boundary Conditions in the Initial AMC Model

In this study, AMC is chosen as the numerical example because most AMCs are periodic structures. Furthermore, AMCs have attracted considerable attention from researchers in recent years. When AMC first emerged, its structure was relatively simple, as shown in Fig. 5. The structure consisted of two parts: a dielectric layer at the bottom and a metal layer on top, with the dimensions clearly marked in Fig. 5. This study utilizes a periodic unit structure combined with periodic thermal boundary conditions to compute the thermal distribution. The thermal results obtained from directly calculating a 64×64 units cell array is used for validation. It was found that the thermal distribution calculated from the 64×64 units cell array closely matches the results obtained from a single unit cell with periodic thermal boundary conditions, as shown in Fig. 6.

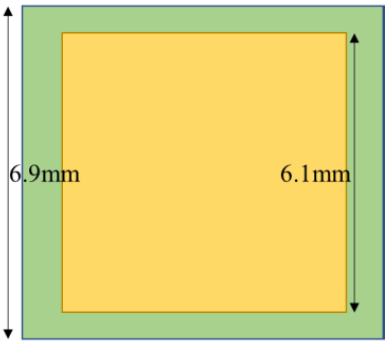

FIGURE 5. The first artificial magnetic conductor model.

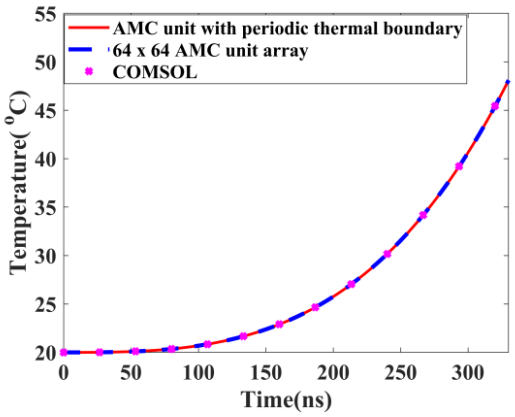

FIGURE 6. The first AMC unit uses periodic thermal boundary conditions and an array of 64×64 units to model temperature variation over time.

3.3. The Latest Thermal Calculations for AMC

In this study, a complex model is used to validate the correctness of the algorithm. The latest AMC model structure still features a dielectric layer at the bottom, but the metal layer now incorporates a complex pattern. As shown in Fig. 7, the metal pattern is symmetrically distributed both vertically and horizontally. The dimensions are also detailed in Fig. 7. In this case,

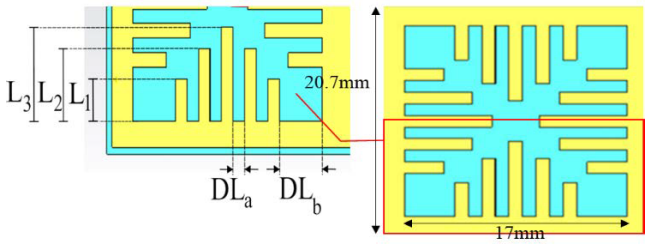

FIGURE 7. The latest artificial magnetic conductor model. $DL_a = 1$, $DL_b = 3.85$, $L_1 = 3$, $L_2 = 5.2$, $L_3 = 6.7$ (unit: mm).

the thermal calculation results of the array composed of 64×64 units are compared with those of the unit structure combined with periodic thermal boundary conditions. The results are in excellent agreement, as shown in Fig. 8.

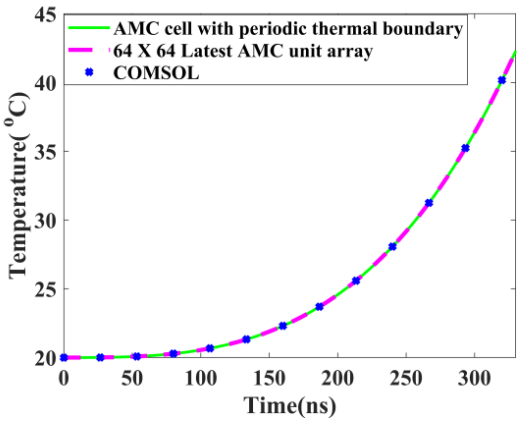

FIGURE 8. The latest AMC unit uses periodic thermal boundary conditions and a 64×64 unit array to model the variation of temperature over time.

3.4. Metasurface Modeling and Simulation

Figure 9 depicts a broadband metasurface, primarily composed of a dielectric substrate with a thickness of 1 mm and a relative permittivity of 4.3, on which metallic patterns are etched to form a basic unit. The design parameters are: $\alpha = 6$ mm, $w = 0.1$ mm, $e = 0.15$ mm, $r1 = 0.75$ mm, $r2 = 1.65$ mm. In this calculation, we first apply periodic thermal boundary conditions to the basic unit shown in Fig. 1 to compute the temperature variation. Next, we calculate the temperature variation of the overall 64×64 array structure. Finally, simulations of the 64×64 array are performed using COMSOL software. The results from all three methods, as shown in Fig. 10, are in excellent agreement, further validating the effectiveness and accuracy of our algorithm.

4. CONCLUSION

This paper presents a novel periodic thermal boundary condition method to address electromagnetic-thermal problems in structures with periodic configurations. By considering electromagnetic losses as the heat source and incorporating the heat conduction equation, a thermal distribution calculation formula applicable to periodic units is successfully derived. The study

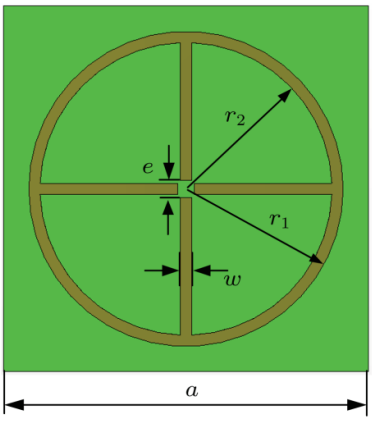

FIGURE 9. Metasurface structure model.

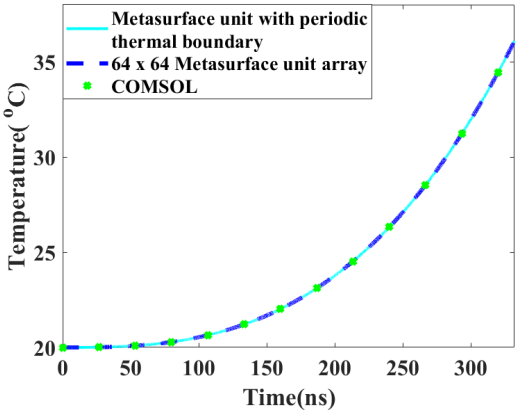

FIGURE 10. The comparison of the temperature-time variation curve of the basic unit of the metasurface combined with periodic thermal boundary conditions and the overall model with a 64×64 array.

demonstrates that this method can accurately predict the temperature distribution of the entire structure through computations performed on a single periodic unit, significantly reducing memory usage and computational time. Numerical experiments validate the accuracy of the proposed method. This research not only enriches the theoretical framework of periodic boundary conditions but also provides an efficient and reliable new approach for solving multiphysics electromagnetic-thermal problems.

ACKNOWLEDGEMENT

This work was supported in part by Anhui Province Higher Education Science Research Project under Grant 2022AH050070; in part by the National Natural Science Foundation of China under Grant 62371002.

REFERENCES

[1] ElMahgoub, K., F. Yang, A. Z. Elsherbeni, V. Demir, and J. Chen, "FDTD analysis of periodic structures with arbitrary skewed grid," *IEEE Transactions on Antennas and Propagation*, Vol. 58, No. 8, 2649–2657, Aug. 2010.

[2] El Mahgoub, K., F. Yang, and A. Z. Elsherbeni, "FDTD/GSM analysis of multilayered periodic structures with arbitrary

skewed grid," *IEEE Transactions on Microwave Theory and Techniques*, Vol. 59, No. 12, 3264–3271, Dec. 2011.

[3] El Mahgoub, K., A. Z. Elsherbeni, and F. Yang, "Dispersive periodic boundary conditions for finite-difference time-domain method," *IEEE Transactions on Antennas and Propagation*, Vol. 60, No. 4, 2118–2122, Apr. 2012.

[4] Ou, N., M. Bai, B. Liang, and J. Miao, "The analysis of periodic structures with 2-D-staggered grid by FDTD algorithm," *IEEE Transactions on Antennas and Propagation*, Vol. 61, No. 1, 290–298, Jan. 2013.

[5] Tekbas, K., F. Costen, J.-P. Bérenger, R. Himeno, and H. Yokota, "Subcell modeling of frequency-dependent thin layers in the FDTD method," *IEEE Transactions on Antennas and Propagation*, Vol. 65, No. 1, 278–286, Jan. 2017.

[6] Zhang, H.-X., Q. Zhan, L. Huang, Y.-D. Wang, W.-J. Wang, Z. Qin, Z.-G. Zhao, D.-W. Wang, H.-J. Zhou, K. Kang, L. Zhou, and W.-Y. Yin, "A scalable HPC-based domain decomposition method for multiphysics modeling of RF devices," *IEEE Transactions on Components, Packaging and Manufacturing Technology*, Vol. 11, No. 12, 2158–2170, 2021.

[7] Xue, Y., Q. Ren, J. Chen, and Y. Zhou, "Transient electromagnetic-thermal cosimulation for micrometer-level components," *IEEE Transactions on Microwave Theory and Techniques*, Vol. 69, No. 10, 4341–4351, 0ct. 2021.

[8] Zhang, H.-X., L. Huang, W.-J. Wang, Z.-G. Zhao, L. Zhou, W. Chen, H. Zhou, Q. Zhan, B. Kolundzija, and W.-Y. Yin, "Massively parallel electromagnetic-thermal cosimulation of large antenna arrays," *IEEE Antennas and Wireless Propagation Letters*, Vol. 19, No. 9, 1551–1555, Sep. 2020.

[9] Lu, T. and J.-M. Jin, "Coupled electrical-thermal-mechanical simulation for the reliability analysis of large-scale 3-D interconnects," *IEEE Transactions on Components, Packaging and Manufacturing Technology*, Vol. 7, No. 2, 229–237, Feb. 2017.

[10] Zhang, H. H., Z. L. Jia, P. F. Zhang, Y. Liu, L. J. Jiang, and D. Z. Ding, "Electromagnetic-circuital-thermal-mechanical multiphysics numerical simulation method for microwave circuits," *IEEE Journal on Multiscale and Multiphysics Computational Techniques*, Vol. 9, 129–141, 2024.

[11] Bui, H. K., F. D. Senghor, G. Wasselynck, D. Trichet, J. Fouladgar, K. Lee, and G. Berthiau, "Characterization of electrical conductivity of anisotropic CFRP materials by means of induction thermography technique," *IEEE Transactions on Magnetics*, Vol. 54, No. 3, 1–4, Mar. 2018.

[12] Kotlan, V., D. Panek, R. Hamar, and I. Dolezel, "Shape optimization of deposited layer produced by combined cladding process," *IEEE Transactions on Magnetics*, Vol. 54, No. 3, 1–4, Mar. 2018.

[13] Jiang, Y., D. Wang, J. Chen, Q. Zhang, and T. Xuan, "Electromagnetic-thermal-fluidic analysis of permanent magnet synchronous machine by bidirectional method," *IEEE Transactions on Magnetics*, Vol. 54, No. 3, 1–5, Mar. 2018.

[14] Wang, J., M. Cheng, W. Qin, and Q. Liu, "Fast calculation method of bi-direction coupling between electromagnetic-thermal field for FSPM motor," *IEEE Transactions on Magnetics*, Vol. 59, No. 12, 1–9, Dec. 2023.

[15] Zhang, H.-X., L. Huang, W.-J. Wang, Z.-G. Zhao, L. Zhou, W. Chen, H. Zhou, Q. Zhan, B. Kolundzija, and W.-Y. Yin, "Massively parallel electromagnetic-thermal cosimulation of large antenna arrays," *IEEE Antennas and Wireless Propagation Letters*, Vol. 19, No. 9, 1551–1555, Sep. 2020.

[16] Zhang, H. H., Z. L. Jia, P. F. Zhang, Y. Liu, L. J. Jiang, and D. Z. Ding, "Electromagnetic-circuital-thermal-mechanical multiphysics numerical simulation method for microwave circuits," *IEEE Journal on Multiscale and Multiphysics Computational Techniques*, Vol. 9, 129–141, 2024.

[17] Wu, S., P. Wang, and Y. Qiao, "Factorization-splitting algorithm based on system incorporated method for periodic nonuniform domains in open regions," *International Journal of Numerical Modelling: Electronic Networks, Devices and Fields*, Vol. 36, No. 6, e3123, 2023.

[18] Lu, Y., J. Chen, J. Li, and W. Xu, "A study on the electromagnetic-thermal coupling effect of cross-slot frequency selective surface," *Materials*, Vol. 15, No. 2, 640, Jan. 2022.